

Electronic Supporting Information

Mössbauer Spectroscopy

Mössbauer spectra were recorded using an alternating constant acceleration *Wissel* Mössbauer spectrometer equipped with a ^{57}Co source in a Rh matrix and operated in transmission mode with a *Janis* closed-cycle helium cryostat for low temperature measurements. Isomer shifts are given relative to α -iron metal at ambient temperature. Simulation of the experimental data was performed using the *Mfit* program (E. Bill, Max-Planck Institute for Bioinorganic Chemistry, Mülheim/Ruhr, Germany).

Mössbauer spectra were recorded between 6 and 260 K to investigate the subtle structural changes associated with the carboxylate shift within the solid state. The powdered crystalline and air-sensitive sample for the Mössbauer experiment was placed in a sealable PEEK-tablet and mounted on a sample holder inside a MBRAUN glovebox with oxygen and water levels below 1 ppm.

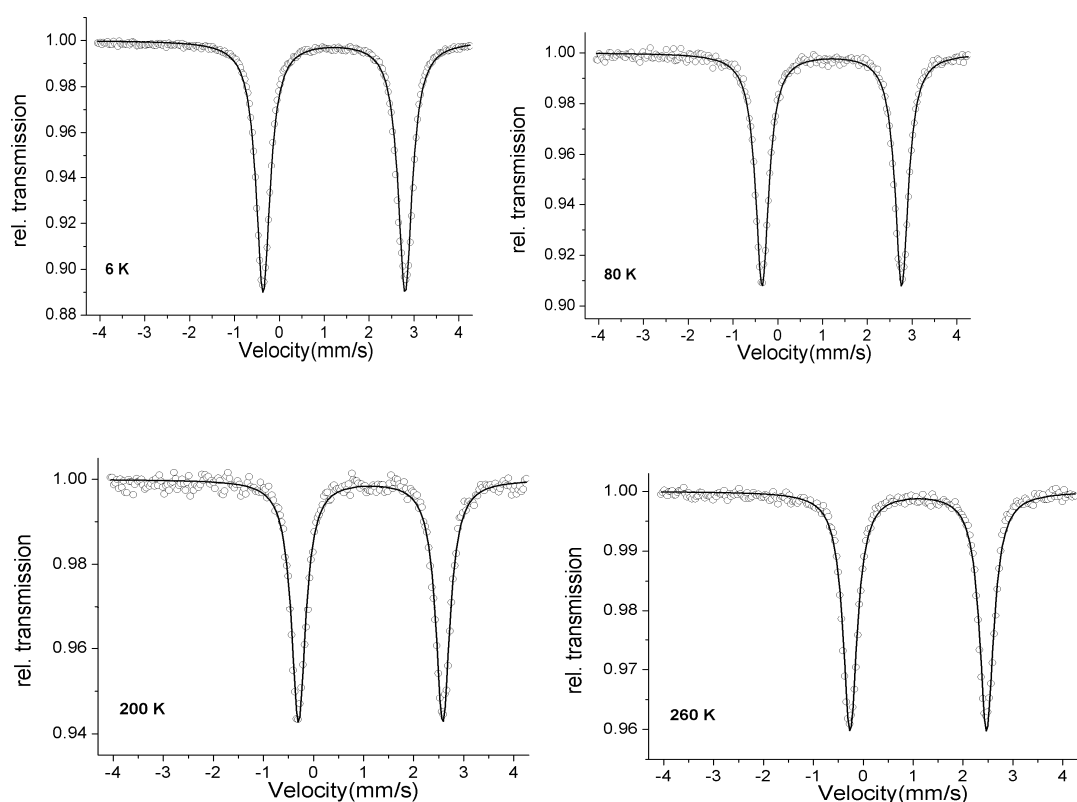


Figure S1 Mössbauer spectra for **1** in the range 6–260 K.

Table S1 Mössbauer Parameters for **1** between 6 and 260 K.

T/K	6	80	200	260
-----	---	----	-----	-----

$\delta_{exp}/(\text{mm/s})$	1.22	1.21	1.14	1.10
$ \Delta E_Q /(\text{mm/s})$	3.17	3.12	2.88	2.74
$\Gamma_{\text{FWHM}}/(\text{mm/s})$	0.38	0.36	0.34	0.34

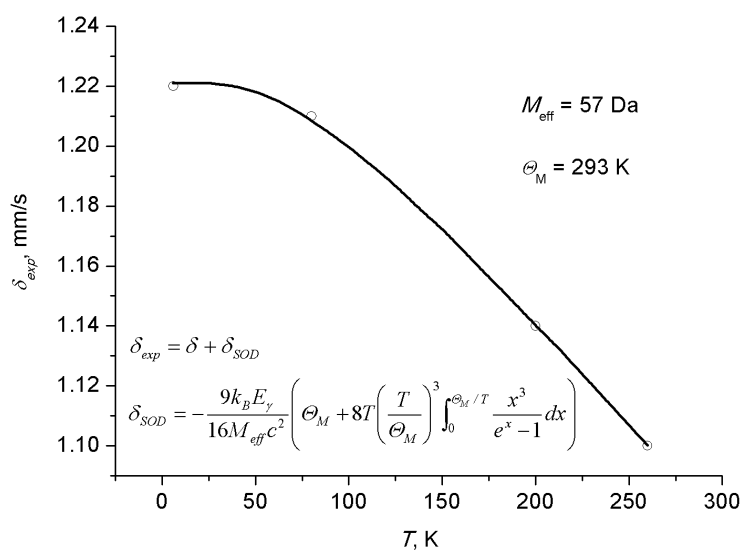


Figure S2 Temperature dependence of the isomer shift for **1** between 6 and 260 K. The temperature dependence of the isomer shift was simulated with the program SOD (E. Bill, Max-Planck Institute for Bioinorganic Chemistry, Mülheim/Ruhr, Germany). The routine is an implementation of Eq. (1) for second-order Doppler shift as given in Ref. 1, which is based on a Debye model for the mean-square velocity of the iron nuclei.¹ The parameters are the Debye temperature Θ_M and the effective mass M_{eff} .

$$\delta_{SOD} = -\frac{9k_B E_\gamma}{16M_{\text{eff}} c^2} \left(\Theta_M + 8T \left(\frac{T}{\Theta_M} \right)^3 \int_0^{\Theta_M/T} \frac{x^3}{e^x - 1} dx \right) \quad \text{Equation (1)}$$

Given that the molecules **1a** and **1b**, and thus the individual Fe centres, become more similar at elevated temperatures (according to their structures) the subtle narrowing of Γ_{FWHM} (see Table S1) with increasing temperature can be explained. This can be also seen by fitting of the Mössbauer spectra with individual subspectra. Due to the distinction of the four iron centres it is reasonable to simulate the Mössbauer spectra with four individual subspectra. We have, however correlated the isomer shifts and line widths of the subspectra to qualitatively assess the anticipated changes in quadrupole splitting. The isomer shifts of all four subspectra have

been set to 1.22 mm/s at 6 K and to 1.10 mm/s at 260 K, which is reasonable with respect to Equation 1 and the findings in Figure S2. After a fitting procedure with variable line widths we fixed an averaged line width of 0.28 mm/s for all four subspectra. This results in four different individual values for quadrupole splittings for the respective iron centres at 6 K. At 260 K it can be clearly seen that the values for quadrupole splittings equilibrate and form two pairs of subspectra that are more similar to each other. In Figure S3 the four individual subspectra at 6 K can be identified by their different color. It is obvious that the set of subspectra at 260 K only shows two colors. This demonstrates that the subspectra are overlayed to a larger extent, meaning the quadrupolar splittings are more similar, which results in a narrower line width at higher temperature.

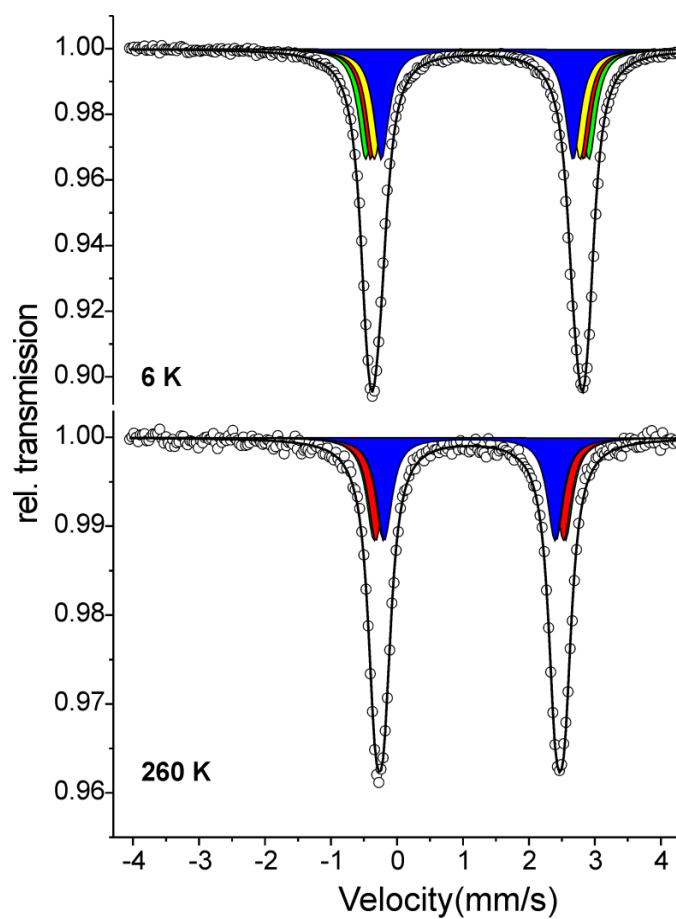


Figure S3 Simulation of the Mössbauer spectra at 6 K and 260 K taking four subspectra into account.

SQUID measurement

Temperature-dependent magnetic susceptibilities were measured using a *Quantum-Design* MPMS-5S SQUID magnetometer equipped with a 5 T magnet, operating in the range from 295 to 2 K. The measurements for **1** were carried out at 5000 Oe. Magnetic properties were simulated using a

Heisenberg-Dirac-van-Vleck Hamiltonian (HDvV) that includes terms for zero-field and Zeeman splitting.²

The sample for SQUID measurement was prepared inside a glovebox and placed in the sample holder using a gelatine capsule under rigorous nitrogen atmosphere.

HDvV operator used for 1

$$\hat{H} = -2J \cdot \hat{\vec{S}}_1 \cdot \hat{\vec{S}}_2 + \sum_i \hat{D}_i (\hat{S}_{z,i}^2 - \frac{1}{3} \hat{S}_i (\hat{S}_i + 1)) + g\mu_B B \sum_i \hat{S}_{z,i}$$

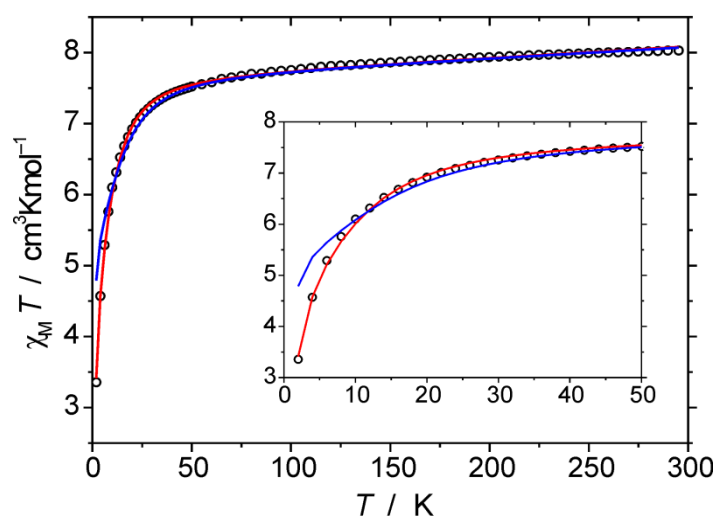


Figure S4: $\chi_M T$ vs. T plot for **1**. The red curve corresponds to the best fit including both zero-field splitting ($|D| = 8.3 \text{ cm}^{-1}$) and antiferromagnetic exchange coupling ($J = -0.07 \text{ cm}^{-1}$). The blue curve demonstrates that the hypothetical "D-only" case does not give an acceptable fit. Further parameters are identical: $g = 2.26$, $PI = 0.5 \text{ \%}$ (fixed), and $TIP = 15.5 \cdot 10^{-4} \text{ cm}^3 \text{ mol}^{-1}$. Temperature-independent paramagnetism (TIP) and a Curie-behaved paramagnetic impurity (PI) with spin $S = 2$ were included according to $\chi_{\text{calc}} = (1 - PI) \cdot \chi + PI \cdot \chi_{\text{mono}} + TIP$. The susceptibility measurements are in accordance with an all-ferrous high spin state of the compound in the temperature range from 300 K down to 2 K.

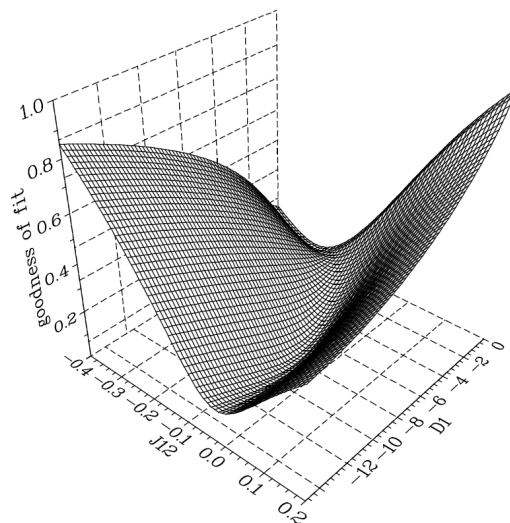


Figure S5: The 3D error surface for the pair J - D .

Experimental Section

The air- and moisture-sensitive compound **1** was manipulated under an atmosphere of purified argon or nitrogen using standard Schlenk- or glovebox-techniques. All solvents were purified and dried according to established procedures and were thoroughly degassed by bubbling with purified Ar prior to use. HL was synthesized from 3,5-bis(chloromethyl)pyrazole³ and bis[2-(1-methylimidazolyl)methyl]-amine⁴ according to the literature method reported earlier⁵. All other chemicals were purchased from commercial sources and used without further purification. Microanalyses were performed by the Analytical Laboratory of the Institute for Inorganic Chemistry of the University of Göttingen.

Synthesis of $[LFe_2(OAc)_3]_2 \cdot 2\text{MeCN}$ (**1**·2MeCN): A solution of HL (1.00 g, 2.0 mmol) in MeCN (100 mL) was treated with KO'Bu (0.24 g, 2.0 mmol). After stirring for several minutes $Fe(OAc)_2$ (0.69 g, 4 mmol) was added. The resulting solution was stirred for 12 hours at room temperature to complete complex formation. Undissolved residues were then filtered off to obtain a clear solution. Colorless single crystals of **1** suitable for x-ray diffraction were grown by slow diffusion of Et_2O into the MeCN solution. Yield(crystalline): 67 %. MS (ESI+, MeCN): $m/z = 731.2 [LFe_2OAc_2]^+$, 617.4 $[LFeOAc+H]^+$, 557.5 $[LFe]^+$, 503.5 $[L+H]^+$, 336.3 $[LFe_2OAc]^{2+}$ Elemental Analysis Calcd. (%) for $C_{31}H_{42}Fe_2N_{12}O_6$: C 47.10, H 5.36, N 21.26. Found: C 47.52, H 5.54, N 21.34.

IR spectroscopy

IR spectra in chloroform were measured using a *Mettler-Toledo* FTIR ReactIR iC10 spectrometer. The spectra at RT (light blue) and at -40°C (dark yellow) are shown below. No dynamic behaviour could be observed in solution.

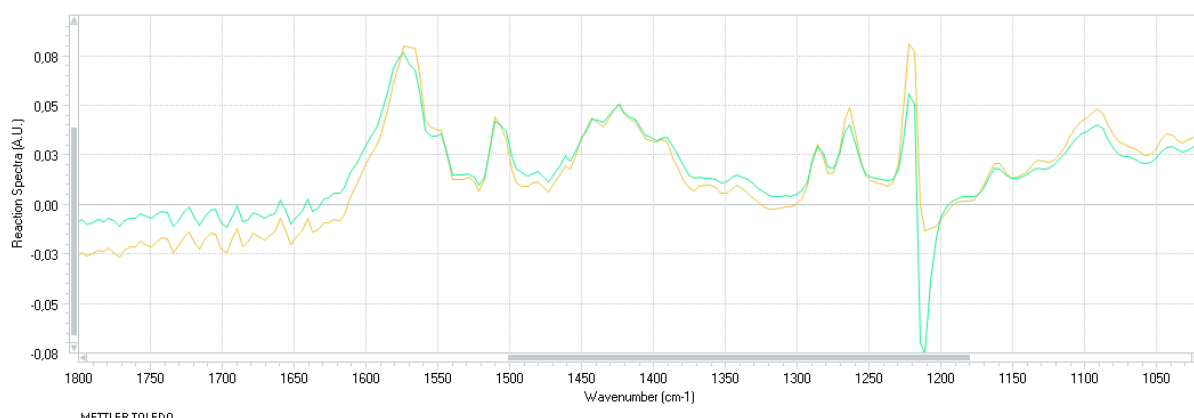


Figure S6 IR spectra of **1** in CHCl_3 at RT (light blue) and at -40°C (dark yellow)

IR spectra of solid **1** have been recorded as KBr pellets at ambient temperature using a *Varian Digilab Excalibur FTS 3000* spectrometer. IR (KBr): $\tilde{\nu}$ (cm^{-1}) = 3117 (m), 2921 (m), 2850 (w), 2362 (w), 2246 (w), 1599 (vs), 1580 (vs), 1504 (s), 1422 (vs), 1328 (m), 1281 (m), 1263 (m), 1143 (m), 1086 (m), 1056 (m), 1041 (m), 1015 (m), 954 (m), 877 (w), 798 (m), 742 (m), 667 (m), 619 (w). The complexity, overlay and broadness of the signals in the carboxylate stretching region does not allow an unambiguous assignment of the absorption bands to the corresponding carboxylate binding modes and a correlation to the structure. The expected temperature dependent variations thus cannot be clearly resolved in the IR spectrum. Changes in the spectrum may anyhow be subtle since the differing coordination modes in **1a** (and thus their respective absorption bands) are already present in the spectrum, as they are similar to those found in **1b**.

X-ray Crystallography

X-ray data for **1** were collected on a STOE IPDS II diffractometer with an area detector (graphite monochromated Mo-K α radiation, $\lambda = 0.71073 \text{ \AA}$) by use of ω scans at 133 K and 248 K for two different crystals (Table S3). The two crystals were found to be enantiomeric. The structures were solved by direct methods and refined on F^2 using all reflections with SHELX-97.⁷ Most non-hydrogen atoms were refined anisotropically.

Hydrogen atoms were placed in calculated positions and assigned to an isotropic displacement parameter of 0.08 Å² or 1.5 $U_{\text{eq}}(\text{C})$ (MeCN). One oxygen atom (O14) in **1** at 133 K was found to be disordered over two positions (occupancy factors: 0.791(6) / 0.209(6)) and was refined using an EADP constraint in all cases. In case of **1** at 248 K the same oxygen atom was found to be disordered (occupancy factors: 0.737(6) / 0.263(6)). Additionally two acetate groups (O1, O2, C26, C27 and O5, O6, C30, C31) are disordered over two positions (occupancy factors: 0.796(6) / 0.204(6) and 0.610(10)/0.390(10)). All atoms of disordered parts in **1** at 248 K were refined isotropically.

Furthermore another single crystal of **1** was measured at four different temperatures (same conditions as above, Table S4). The disordered parts are the same as above and were treated in the same way. The occupancy factors are listed in Table S2.

Face-indexed absorption corrections were performed numerically with the program X-RED.⁸

Additionally **1** was flash cooled in liquid nitrogen and a low temperature synchrotron data set was collected at the BESSY ML Beamline 14.2 with a Mar MX-225 detector ($\lambda = 0.800 \text{ \AA}$) at 100 K (Table S5) to confirm the absence of any disorder at low temperature. One oxygen atom (O14) in **1** was found to be disordered over two positions (occupancy factors: 0.874(6) / 0.126(6)) and was refined using an EADP constraint. No further disorder of the acetate ligands was encountered at low temperature. Absorption and intensity data were corrected with the SADABS program.⁹

Table S2 Occupancy factors of the disordered parts in **1** at different temperatures.

disordered part	occupancy factors at			
	271 K	248 K	213 K	133 K
O14	0.736(6) /	0.727(5) /	0.736(5) /	0.828(5) /
	0.264(6)	0.273(5)	0.264(5)	0.172(5)
O1, O2, C26, C27	0.762(6) /	0.806(6) /	0.861(6) /	1
	0.238(6)	0.194(6)	0.139(6)	
O5, O6, C30, C31	0.564(11) /	0.623(10) /	0.717(10) /	1
	0.436(11)	0.377(10)	0.283(10)	

Table S3 Crystal data and structure refinement for **1** (two different crystals, enantiomorphous) at 248 K (left) and 133 K (right).

empirical formula	C ₃₅ H ₄₈ Fe ₂ N ₁₄ O ₆
-------------------	--

formula weight	872.57	
crystal size [mm ³]	0.41 × 0.20 × 0.18	0.40 × 0.36 × 0.28
crystal system	Orthorhombic	
space group	<i>P</i> 2 ₁ 2 ₁ 2 ₁ (No. 19)	
<i>a</i> [Å]	16.3776(3)	16.2959(3)
<i>b</i> [Å]	19.0030(4)	18.9302(3)
<i>c</i> [Å]	26.5500(7)	26.2922(5)
$\alpha = \beta = \gamma$ [°]		90
<i>V</i> [Å ³]	8263.0(3)	8110.7(3)
<i>Z</i>		8
ρ [g/cm ³]	1.403	1.429
<i>F</i> (000)	3648	3648
μ [mm ⁻¹]	0.763	0.777
<i>T</i> _{min} / <i>T</i> _{max}	0.7110 / 0.8454	0.7186 / 0.8421
θ range [°]	1.32 - 26.82	1.33 - 26.76
<i>hkl</i> range	±20, ±24, ±33	±20, ±23, ±33
measured refl.	96951	76329
unique refl. [<i>R</i> _{int}]	17574 [0.0480]	17205 [0.0404]
observed refl. (<i>I</i> > 2σ(<i>I</i>))	14817	16628
data / restraints / param.	17574 / 0 / 1023	17205 / 0 / 1046
goodness-of-fit (<i>F</i> ²)	1.044	1.139
Abs. structure parameter	0.014(10)	0.024(8)
<i>R</i> 1, <i>wR</i> 2 (<i>I</i> > 2σ(<i>I</i>))	0.0411, 0.0916	0.0353, 0.0841
<i>R</i> 1, <i>wR</i> 2 (all data)	0.0533, 0.0953	0.0371, 0.0847
resid. el. dens. [e/Å ³]	-0.586 / 0.496	-0.434 / 0.617

Table S4 Crystal data and structure refinement for **1** (one crystal) at different temperatures.

empirical formula	C ₃₅ H ₄₈ Fe ₂ N ₁₄ O ₆			
formula weight	872.57			
crystal size [mm ³]	0.40 × 0.30 × 0.24			
crystal system	Orthorhombic			
space group	<i>P</i> 2 ₁ 2 ₁ 2 ₁ (No. 19)			
<i>T</i> [K]	271	248	213	133
<i>a</i> [Å]	16.4147(4)	16.3877(4)	16.3489(3)	16.2919(4)
<i>b</i> [Å]	19.0401(5)	19.0209(4)	18.9892(4)	18.9469(4)
<i>c</i> [Å]	26.6275(6)	26.5783(6)	26.4822(5)	26.2523(5)
$\alpha = \beta = \gamma$ [°]			90	
<i>V</i> [Å ³]	8322.1(4)	8284.7(3)	8221.5(3)	8103.6(3)

Z	8			
ρ [g/cm ³]	1.393	1.399	1.410	1.430
F(000)	3648	3648	3648	3648
μ [mm ⁻¹]	0.758	0.761	0.767	0.778
T_{\min}/ T_{\max}	0.7807 / 0.8668	0.7817 / 0.8669	0.7708 / 0.8482	0.7661 / 0.8496
Θ range [°]	1.31 - 25.71	1.32 - 25.71	1.32 - 25.69	1.33 - 26.83
<i>hkl</i> range				
	-19 - 20	-19 - 20	±19	±20
	-22 - 23	-22 - 23	-22 - 23	±23
	±33	±33	±32	±33
measured refl.	96150	98806	94982	78904
unique refl. [R_{int}]	15791 [0.0617]	15703 [0.0586]	15577 [0.0571]	17246 [0.0604]
obs. refl. ($I > 2\sigma(I)$)	13086	13393	13923	15179
data / restr. / param.	15791 / 0 / 1032	15703 / 0 / 1032	15577 / 0 / 1032	17246 / 0 / 1045
goodness-of-fit (F^2)	1.005	1.005	1.001	1.004
Abs. structure param.	0.010(10)	0.024(8)	0.011(8)	0.003(7)
$R_1, wR_2 (I > 2\sigma(I))$	0.0408, 0.0910	0.0379, 0.0793	0.0352, 0.0786	0.0352, 0.0690
R_1, wR_2 (all data)	0.0531, 0.0946	0.0480, 0.0820	0.0420, 0.0806	0.0440, 0.0710
resid. el. dens. [e/Å ³]	-0.345 / 0.512	-0.337 / 0.597	-0.352 / 0.589	-0.285 / 0.493

Table S5 Crystal data and structure refinement for **1** (synchrotron radiation at 100 K)

empirical formula	C ₃₅ H ₄₈ Fe ₂ N ₁₄ O ₆
formula weight	872.57
crystal size [mm ³]	0.40 × 0.40 × 0.30
crystal system	Orthorhombic
space group	P2 ₁ 2 ₁ 2 ₁ (No. 19)
a [Å]	16.264(3)
b [Å]	18.940(4)
c [Å]	26.215(5)
$\alpha = \beta = \gamma$ [°]	90
V [Å ³]	8075(3)
Z	8
ρ [g/cm ³]	1.435
F(000)	3648
μ [mm ⁻¹]	0.781
T_{\min}/ T_{\max}	0.6983 / 0.7461
Θ range [°]	1.49 - 30.92

<i>hkl</i> range	$\pm 20, \pm 24, -33 - 32$
measured refl.	62244
unique refl. [<i>R</i> _{int}]	17697 [0.0324]
observed refl. (<i>I</i> > 2σ(<i>I</i>))	16890
data / restraints / param.	17697 / 0 / 1045
goodness-of-fit (<i>F</i> ²)	1.034
Abs. structure parameter	-0.079(7)
<i>R</i> 1, <i>wR</i> 2 (<i>I</i> > 2σ(<i>I</i>))	0.0340, 0.0849
<i>R</i> 1, <i>wR</i> 2 (all data)	0.0359, 0.0860
resid. el. dens. [e/Å ³]	-0.612 / 1.174

Table S6: Selected bond lengths [Å] for **1** (all data were collected from the same crystal, except the synchrotron measurements which were collected from an enantiomeric crystal)

atoms	271K	248K	213K	133K	Syncrotron 100K
Fe1-N1	2.105(2)	2.112(2)	2.111(2)	2.116(2)	2.1221(19)
Fe1-N4	2.103(3)	2.109(2)	2.115(2)	2.124(2)	2.1253(19)
Fe1-O3	2.157(3)	2.168(2)	2.177(2)	2.1919(18)	2.1927(16)
Fe1-N6	2.174(3)	2.179(3)	2.180(2)	2.189(2)	2.1881(19)
Fe1-O1(A)	2.267(4)	2.251(3)	2.224(3)	2.1893(18)	2.1852(18)
Fe1-N3	2.6827(26)	2.6913(24)	2.7040(22)	2.7265(20)	2.7261(19)
Fe1-O4	2.4251(29)	2.4186(25)	2.4086(22)	2.3934(19)	2.3924(18)
Fe2-O6A	2.305(6)	2.302(5)	2.291(4)	2.266(2)	2.2660(17)
Fe2-O6(B)	1.991(10)	2.013(11)	2.071(13)		
Fe2-O2(A)	1.998(4)	2.013(3)	2.031(3)	2.0516(19)	2.0541(18)
Fe2-N2	2.130(3)	2.134(2)	2.135(2)	2.131(2)	2.1296(18)
Fe2-N9	2.206(3)	2.207(3)	2.203(2)	2.198(2)	2.195(2)
Fe2-O3	2.244(2)	2.238(2)	2.2337(19)	2.2321(17)	2.2286(16)
Fe2-O5(A)	2.255(6)	2.241(5)	2.222(4)	2.214(2)	2.2047(18)
Fe2-O1(B)	2.269(12)	2.253(14)	2.238(19)		
Fe11-N21	2.066(3)	2.071(2)	2.068(2)	2.069(2)	2.0776(19)
Fe11-O11	2.079(2)	2.080(2)	2.081(2)	2.0887(18)	2.0915(16)
Fe11-N26	2.081(3)	2.082(2)	2.085(2)	2.085(2)	2.080(2)
Fe11-N24	2.090(3)	2.088(3)	2.085(3)	2.084(2)	2.084(2)
Fe11-N23	2.5528(30)	2.5525(27)	2.5499(24)	2.5490(21)	2.5532(19)
Fe11-O12	2.6176(30)	2.6140(27)	2.6076(24)	2.5819(19)	2.5701(19)
Fe12-O13	1.994(3)	1.997(2)	1.999(2)	2.0097(19)	2.0108(18)
Fe12-N22	2.108(3)	2.111(2)	2.111(2)	2.115(2)	2.1144(19)
Fe12-O15	2.161(3)	2.161(2)	2.161(2)	2.163(2)	2.1669(17)
Fe12-O16	2.4276(34)	2.4257(29)	2.4187(24)	2.4017(21)	2.4005(19)
Fe12-N29	2.202(3)	2.197(2)	2.197(2)	2.190(2)	2.188(2)
Fe12-O11	2.328(2)	2.321(2)	2.3066(19)	2.2797(16)	2.2710(16)

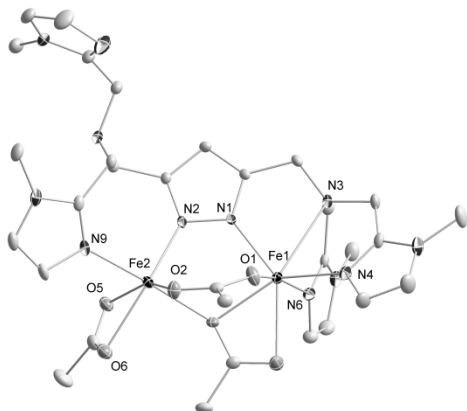


Figure S7a. Molecular structure of **1a** @ 133K as diamond plot. Displacement ellipsoids at 30% probability Selected bond lengths [Å] and angles [°] for **1a**: Fe1-N1 2.114(2), Fe1-N4 2.116(2), Fe1-N6 2.183(2), Fe1-O3 2.1875(18), Fe1-O1 2.191(2), Fe1-O4 2.386(2), Fe2-O2 2.047(2), Fe2-N2 2.129(2), Fe2-N9 2.195(2), Fe2-O5 2.211(2), Fe2-O3 2.2257(18), Fe2-O6 2.261(2), N1-Fe1-N4 125.41(8), N1-Fe1-N6 102.75(8), N4-Fe1-N6 92.48(9), N1-Fe1-O3 84.89(7), N4-Fe1-O3 146.05(8), N6-Fe1-O3 95.20(7), N1-Fe1-O1 89.35(8), N4-Fe1-O1 81.59(8), N6-Fe1-O1 167.80(9), O3-Fe1-O1 84.16(7), N1-Fe1-O4 141.84(7), N4-Fe1-O4 90.69(8), N6-Fe1-O4 85.70(8), O3-Fe1-O4 57.13(7), O1-Fe1-O4 83.73(8), O2-Fe2-N2 108.73(8), O2-Fe2-N9 86.75(8), N2-Fe2-N9 100.67(8), O2-Fe2-O5 155.39(8), N2-Fe2-O5 95.65(8), N9-Fe2-O5 92.19(8), O2-Fe2-O3 87.58(7), N2-Fe2-O3 84.16(7), N9-Fe2-O3 173.50(8), O5-Fe2-O3 91.65(7), O2-Fe2-O6 96.66(8), N2-Fe2-O6 153.67(8), N9-Fe2-O6 87.32(8), O5-Fe2-O6 58.73(8), O3-Fe2-O6 90.20(7).

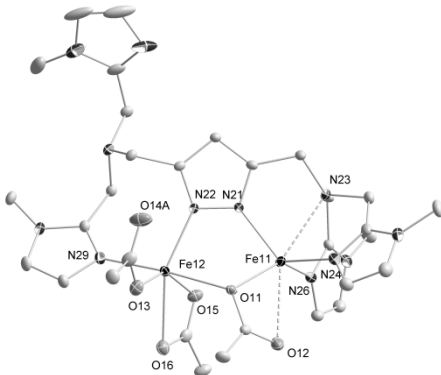


Figure S7b. Molecular structure of **1b** @ 133K as diamond plot. Displacement ellipsoids at 30% probability. Selected bond lengths [Å] and angles [°] for **1b**: Fe11-N21 2.069(2), Fe11-N26 2.079(2), Fe11-O11 2.0805(18), Fe11-N24 2.081(2), Fe12-O13 2.0057(19), Fe12-N22 2.112(2), Fe12-O15 2.1575(19), Fe12-N29 2.188(2), Fe12-O11 2.2794(17), Fe1-Fe2 3.6082(5), Fe11-Fe12 3.5213(5); C66-O11-Fe11 102.72(16), C66-O11-Fe12 125.07(15), Fe11-O11-Fe12 107.65(7), C68-O13-Fe12 121.48(19), C70-O15-Fe12 96.33(17), N21-Fe11-N26 113.57(9), N21-Fe11-O11 85.66(8), N26-Fe11-O11 135.66(8), N21-Fe11-N24 118.77(9), N26-Fe11-N24 101.33(9), O11-Fe11-N24 103.04(8), O13-Fe12-N22 120.82(8), O13-Fe12-O15 145.24(8), N22-Fe12-O15 91.51(8), O13-Fe12-N29 91.22(9), N22-Fe12-N29 99.10(8), O15-Fe12-N29 96.18(8), O13-Fe12-O11 88.07(8), N22-Fe12-O11 84.58(7), O15-Fe12-O11 82.25(7), N29-Fe12-O11 176.06(7).

In Figures S7a and S7b the structures of molecules **1a** and **1b** measured @133K are depicted along with some selected metrical data. The crystal used was enantiomeric to the one used for collection of the data for the main paper (in range 133 K - 271 K), thus the two molecules shown in Figures S7a and S7b are enantiomers of the molecules shown in the main paper.

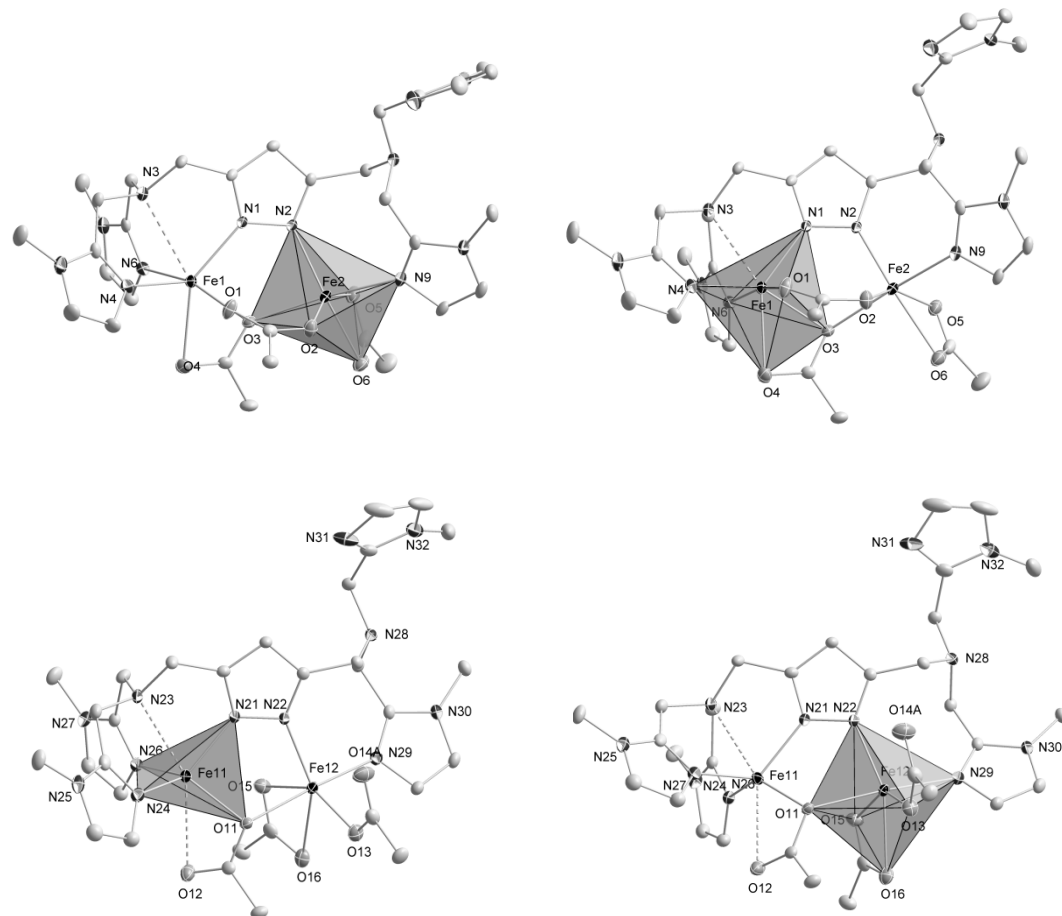


Figure S8 Representation of the individual coordination polyhedra for **1a** (top) and **1b** (bottom). In **1a** the coordination polyhedron for Fe2 (upper left) can be described as a distorted octahedron with a $\{N_2O_4\}$ -donor set. The coordination polyhedron for Fe1 (upper right) is better described as a fairly distorted octahedron having one face capped by an additional aliphatic nitrogen donor, resulting in a $\{N_3O_3(N)\}$ donor set. In **1b** Fe12 exhibits a $\{N_2O_4\}$ -donor set forming a distorted octahedron (lower right) comparable to Fe2. The ligating environment of Fe11 is better described as a distorted $\{N_3O\}$ tetrahedron (lower left) with two of the faces capped by one oxygen donor of an acetate ligand and an aliphatic nitrogen donor of the ligand backbone, resulting in an overall $\{N_3O(NO)\}$ donor set.

References

1. P. Gütlich, E. Bill and A. X. Trautwein, *Mössbauer Spectroscopy and Transition Metal Chemistry*, Springer, Heidelberg, 2011.

2. Full-matrix diagonalization of exchange coupling and Zeeman splitting was performed with the *julX* program (E. Bill, Max Planck Institute for Bioinorganic Chemistry, Mülheim/Ruhr, Germany).
3. T. G. Schenck, J. M. Downes, C. R. C. Milne, P. B. Mackenzie, T. G. Boucher, J. Whelan, B. Bosnich, *Inorg. Chem.* 1985, **24**, 2334-2337.
4. K. J. Oberhausen, J. F. Richardson, R. M. Buchanan, W. Pierce, *Polyhedron* 1989, **8**, 659-668.
5. A. Prokofieva, A. I. Prikhod'ko, E. A. Enyedy, E. Farkas, W. Maringgele, S. Demeshko, S. Dechert, F. Meyer, *Inorg. Chem.* 2007, **46**, 4298-4307.
6. V. Robert and G. Lemercier, *J. Am. Chem. Soc.*, 2006, **128**, 1183-1187.
7. G. M. Sheldrick, *Acta Crystallogr.*, 2008, **A64**, 112–122.
8. STOE & CIE GmbH, X-RED, Darmstadt, Germany, 2002.
9. G. M. Sheldrick, SADABS, Program for Empirical Absorption Correction of Area Detector Data, University of Göttingen, Göttingen, Germany, 2009.